Journal of Geodesy (1997) 71: 113–130

Journal of Geodesy

© Springer-Verlag 1997

Analysis of some systematic errors affecting altimeter-derived sea surface gradient with application to geoid determination over Taiwan

C. Hwang

Department of Civil Engineering, National Chiao Tung University, 1001 Ta Hsueh Road, Hsinchu 30050, Taiwan, ROC.

Received 22 January 1996; Accepted 13 September 1996

Abstract. This paper analyzes several systematic errors affecting sea surface gradients derived from Seasat, Geosat/ERM, Geosat/GM, ERS-1/35d, ERS-1/GM and TOPEX/POSEIDON altimetry. Considering the data noises, the conclusion is: (1) only Seasat needs to correct for the non-geocentricity induced error, (2) only Seasat and Geosat/GM need to correct for the one cycle per revolution error, (3) only Seasat, ERS-1/GM and Geosat/GM need to correct for the tide model error; over shallow waters it is suggested to use a local tide model not solely from altimetry. The effects of the sea surface topography on gravity and geoid computations from altimetry are significant over areas with major oceanographic phenomena. In conclusion, sea surface gradient is a better data type than sea surface height. Sea surface gradients from altimetry, land gravity anomalies, ship gravity anomalies and elevation data were then used to calculate the geoid over Taiwan by least-squares collocation. The inclusion of sea surface gradients improves the geoid prediction by 27% when comparing the GPS-derived and the predicted geoidal heights, and by 30% when comparing the observed and the geoid-derived deflections of the vertical. The predicted geoid along coastal areas is accurate to 2 cm and can help GPS to do the third-order leveling.

Introduction

Altimetry has made an important contribution to marine geophysics as the increasingly dense altimeter data are being used to derive the marine gravity and the marine geoid with unprecedented resolutions and accuracies. With altimeter data from the newly completed ERS-1/GM and the newly released global Geosat/GM (Carlowicz 1995) more discoveries are foreseen. In these derivations the used altimeter data type is either sea surface height (SSH) or sea surface gradient (SSG). Both SSH and SSG are subject to errors. While the errors in SSH and the methods for reducing or modeling such errors have been extensively discussed, e.g., Tapley et al. (1982), Knudsen (1991) and Shum et al. (1995), the errors in SSG receive only little attention, e.g., Sandwell and Zhang (1989). One usually asserts that the use of SSG will mitigate many problems in the altimeter data, especially the orbit error, thus SSG is considered a better data type than SSH, see, e.g., Haxby et al. (1982), Sandwell (1992), McAdoo and Marks (1992), Hwang and Parsons (1995, 1996), and Hwang (1996). Although there is no direct proof of this assertion, the comparison made by Olgiati et al. (1995) indeed shows that the predicted gravity anomalies from using SSG yields a better agreement with ship gravity than from using SSH. Here a SSG, e, is defined as the gradient of along-track SSH, h

$$e(\alpha) = \frac{\partial h}{\partial s}\,, \tag{1}$$

where s is the along-track distance and α is the azimuth of the gradient. In the first part of this paper we will discuss several errors affecting SSG and the consequences. Due to the presence of the sea surface topography (SST), in fact the sea surface does not coincide with the marine geoid and we will also discuss the effect of neglecting the SST in using SSG to derive the functionals of the earth's disturbing potential. To do this we obtained existing Seasat, Geosat, ERS-1 and TOPEX/POSEIDON (T/P) altimeter data from some major institutions. Table 1 shows the informations of interest. The noise of SSH in Table 1 is obtained by dividing the instrument noise (Shum et al. 1995) by the square root of the number of cycles for averaging. This estimate is only approximate because we have neglected data gaps at repeat cycles. In order to compare the magnitudes of the various errors affecting SSG, as well as the magnitude of SST gradient, the estimated noises of SSG are also included in Table 1. The noise of a SSG is derived from the simple formula $\sqrt{2}\sigma/d$, where σ is the noise of SSH and d is the average data spacing between two successive points of 1 per second altimeter data

Table 1. Satellite altimeter data used for error analysis and geoid determination

Satellite mission	Data sources	Ave. cycles and period	Instrument noise of SSH[a] (cm)	Estimated noise of SSG (μrad)	Semimajor axis (m)	Reference
Seasat	OSU[b]	–	5.0	10.5	6378137	Rapp (1982)
Geosat/ERM[c]	OSU[b]	22,1 yr	1.1	2.2	6378136.3	Wang and Rapp (1992)
Geosat/GM[d]	NOAA	–	5.0	10.5	6378137	Cheney et al. (1991)
ERS-1/35d[e]	CERSAT	18, 1.5 yr	0.7	1.5	6378137	Dumont and Stum (1994)
ERS-1/GM[d]	NOAA	–	3.0	6.3	6378137	Cheney and Lillibridge (1992)
T/P	AVISO	36, 1yr	0.3	0.7	6378136.3	AVISO (1992)

[a] Sampling rate is 1 HZ
[b] The Ohio State University
[c] Geosat with 17-day repeat period
[d] Geodetic mission
[e] ERS-1 with 35-day repeat period

(Hwang and Parsons 1995). Furthermore, the flattening of the reference ellipsoid is 1/298.257 for the SSH from all satellite missions.

Another objective of this study is to determine the geoid over Taiwan using altimeter-derived SSG and gravity data. Taiwan is an island with a dimension of 2° west-east and 5° north-south. The role of altimeter data in geoid determination over an island is to fill the data gap at sea, thus altimeter data contribute important information to the coastal geoid. In fact the direct or the indirect approach can be used when incorporating altimeter data into geoid computations. In the direct approach altimeter-derived SSH or SSG and gravity anomalies are used simultaneously to determine the geoid, while in the indirect approach SSH or SSG are first converted to gravity anomalies which are then merged with measured gravity anomalies to determine the geoid. For the direct approach, since the data used are heterogeneous the only technique for this purpose is least-squares collocation (LSC) (Moritz 1980). For the indirect approach, LSC can still be used but since the data are homogeneous a FFT method is preferred if one wishes to reduce the computational time. Furthermore, the indirect approach will introduce additional errors from data type conversion and, if a FFT method is used, from data gridding. In this paper LSC together with the RTM method (Forsberg 1984) will be adopted for the geoid determination over Taiwan. The computed geoid will be compared with GPS-derived geoidal heights and its gradient will be compared with astrogeodetic deflections of the vertical.

Systematic errors affecting altimeter-derived sea-surface gradients

Non-geocentricity induced error

The accuracy of a satellite's ellipsoidal height, and consequently the accuracy of SSH, depends in part on the terrestrial reference frame in which the orbits are determined (Shum et al. 1995; Hwang 1995). If the satellite's terrestrial reference frame is not geocentric, an altimeter-derived SSH, ζ, will deviate from the SSH referring to the geocentric frame, ζ_0, in the form (Rapp 1989):

$$\zeta = \zeta_0 + \cos\phi\cos\lambda\Delta x + \cos\phi\sin\lambda\Delta y + \sin\phi\Delta z - W\Delta a + \frac{a_S(1-f_S)}{W}\sin^2\phi\Delta f \ , \tag{2}$$

where ϕ and λ are geodetic latitude and longitude, respectively, a_S and f_S are the semi-major axis and the flattening of the reference ellipsoid for the satellite's geodetic system, Δx, Δy and Δz are three translation parameters, $W = \sqrt{1-e^2\sin^2\phi}$ with $e^2 = 2f_S - f_S^2$, and $\Delta a = a_I - a_S$, $\Delta f = f_I - f_S$ with a_I and f_I being the semi-major axis and the flattening of some "best" ellipsoid. Considering the "best" ellipsoid is that used in the T/P reference frame, we have a_I=6378136.3 m, and f_I=1/298.257. Table 1 also lists the semi-major axes of the ellipsoids for the altimeter data used in this paper. Since the reference ellipsoids are known, the effect due to Δa and Δf may be removed before comparing SSH in two satellite frames. Within the same satellite frame, the three translations are unobservable in crossover differences of SSH and hence cannot be removed by crossover adjustments of SSH. The SSH error due to Δz is also aliased with the one cycle per revolution orbit error (Hwang 1995). It is also clear that the effect of non-geocentricity cannot be removed by averaging data from repeat cycles.

After removing the effects due to Δa and Δf, the errors in the north and the east components of SSG due to the non-geocentricity of the reference frame can be calculated by

$$\Delta\varepsilon_y = \frac{\partial(\zeta-\zeta_0)}{\partial y} = \frac{\partial(\zeta-\zeta_0)}{R\partial\phi} = -\frac{\Delta x}{R}\sin\phi\cos\lambda - \frac{\Delta y}{R}\sin\phi\sin\lambda + \frac{\Delta z}{R}\cos\phi \ , \tag{3}$$

and

$$\Delta\varepsilon_x = \frac{\partial(\zeta-\zeta_0)}{\partial x} = \frac{\partial(\zeta-\zeta_0)}{R\cos\phi\,\partial\lambda} = -\frac{\Delta x}{R}\sin\lambda + \frac{\Delta y}{R}\cos\lambda \ , \tag{4}$$

where x, y are the local horizontal coordinates and R is the earth's mean radius (~ 6371 km). To get the error in

an along-track SSG with azimuth α, one can use the formula

$$\Delta\,\varepsilon_\alpha = \Delta\varepsilon_x \cos\,\alpha + \Delta\varepsilon_y \sin\,\alpha\ . \tag{5}$$

To see the maximum effects, we may set to zeroes the partial derivatives of $\Delta\epsilon_x$ and $\Delta\epsilon_y$ with respect to ϕ and λ separately, leading to:

$$\text{Maximum } \Delta\varepsilon_x = \frac{\sqrt{\Delta x^2 + \Delta y^2}}{R}, \text{when} \tan\lambda = \frac{-\Delta x}{\Delta y}, \tag{6}$$

and

$$\text{Maximum } \Delta\varepsilon_y = \frac{\sqrt{\Delta x^2 + \Delta y^2 + \Delta z^2}}{R}, \quad \text{when } \tan\,\lambda = \frac{\Delta x}{\Delta y} \quad \text{and} \tan\phi = \frac{-\sqrt{\Delta x^2 + \Delta y^2}}{\Delta z} \tag{7}$$

Assuming that the T/P reference frame is geocentric, it is possible to find the three translations for each of the satellite frames using the crossover differences $(\zeta - \zeta_0)$ between the T/P SSH and the SSH from a satellite mission. To reduce the computational time while having globally distributed data, for each participating satellite we selected about 254 passes to form crossovers with the 254 passes of T/P over $-66°<$latitude$<66°$. The Geosat/GM data available to the author covers only the area south of 30°S so the corresponding translations cannot be determined due to the poor geometry for parameter estimation. Figure 1 shows the crossover differences between T/P and other satellite missions (excluding Geosat/GM). It was found that T/P-T/P rms crossover difference is 0.08 m and is consistent with the 4-cm orbit accuracy (Tapley et al. 1994) if other errors are counted. Note that the number 0.08 cm is based on all T/P-T/P crossovers, while some authors, e.g. Tai and Kuhn (1994), used T/P-T/P crossovers only over waters with depth greater than 1000 m. Large T/P-Seasat crossover differences exist over most of the Indian Ocean, the Central-South Pacific and most of the South Atlantic. The T/P-Geosat/ERM crossover differences over the Western Pacific and the Northern Indian Ocean are also quite large. The T/P-ERS-1/35d and T/P-ERS-1/GM crossover differences are quite uniform globally, but clearly some ERS-1/35d and ERS-1/GM passes contain bad data.

For each crossover difference we can write the observation equation as

$$(\zeta - \zeta_0) + v = \cos\,\phi\cos\lambda\Delta x + \cos\phi\,\sin\,\lambda\Delta y + \sin\phi\Delta_z\ , \tag{8}$$

where the residual v in fact contains both random noises and systematic errors such as orbit errors (if any) from T/P and the participating satellite. The translations $\Delta x, \Delta y$ and Δz were then solved by the least-squares method which minimizes the sum of the squared residuals. Table 2 shows the results. Note that in Table 2 we used only those crossover differences passing the simple 3σ outlier rejection criterion because the anomalously large crossover differences (for ERS-1/GM some as large as 32 m) will bias the solutions. Geosat/GM's reference frame is WGS84 (Cheney et al. 1991, p.27) so there will be no translations for Geosat/GM if one assumes that the WGS84 system is geocentric. It is clear from Table 2 that the maximum effects of the translations on SSG derived from Geosat/ERM, ERS-1/35d and ERS-1/GM are rather small compared to their instrument noises listed in Table 1. The maximum effect on Seasat's SSG has a notable 0.129 μrad, but is still considered small compared to its 10.5 μrad instrument noise. According to (4) and (5) a Seasat-derived along-track SSG should be corrected by $-0.129\cos\phi\,\sin\alpha$. Furthermore, the root-mean-squared (rms) crossover differences after applying the translations decrease only marginally and this implies that other errors exist in the altimeter SSH.

One cycle per revolution error

In the previous section we have obtained the rms a *posteriori* crossover differences after eliminating the translations, which are useful for estimating the orbit errors. The within-satellite rms crossover differences for Seasat, Geosat/ERM, ERS-1/35d, ERS-1/GM are 0.22 m, 0.19 m, 0.16 m, and 0.25 m, respectively, which are smaller than the *a posteriori* cross-satellite rms crossover differences listed in Table 2. Assuming that T/P is free from geographically correlated orbit error and neglecting other errors such as ocean tides, the inconsistency between the within-satellite and the cross-satellite rms crossover differences indicates that geographically correlated orbit errors exist in the satellite data other than T/P (note that, when forming the within-satellite crossover differences such orbit errors are canceled). In fact, if T/P is orbit error-free, then Figure 1 shows the full spectra of orbit errors of other satellites. Furthermore, it is known that in most cases the largest component of the orbit errors is the one with the frequency of one cycle per revolution (cpr) (Engelis 1987). The one cpr orbit error may be expressed as

$$\Delta r = a\cos\,(\omega t + \theta_0)\ , \tag{9}$$

Table 2. Results of solving three translations from a satellite's reference frame to T/P's reference frame and the maximum errors in sea surface gradient due to translations

Satellite mission	Rms before (m)	Rms after (m)	Δx (m)	Δy (m)	Δz (m)	Max $\Delta\varepsilon_x$ (μrad)	Max $\Delta\varepsilon_y$ (μrad)
Seasat	0.81	0.75	0.02	0.02	−0.82	0.004	0.129
Geosat/ERM	0.38	0.35	−0.10	0.10	−0.31	0.022	0.053
ERS-1/35d	0.24	0.23	0.07	0.06	0.11	0.014	0.023
ERS-1/GM	0.47	0.44	0.07	0.04	0.31	0.013	0.050

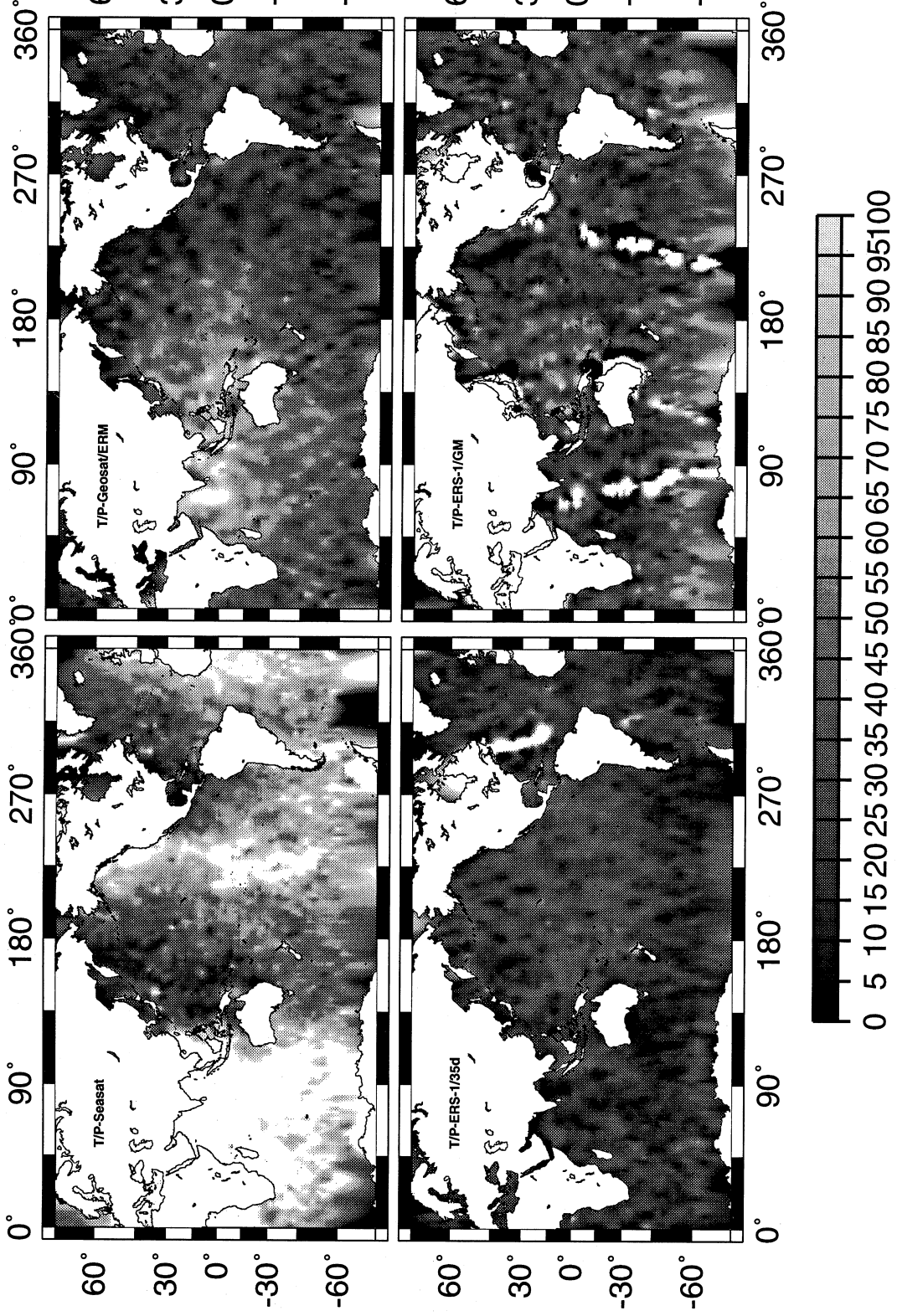

Fig. 1. Crossover differences of sea surface heights between TOPEX/POSEIDON and other satellite missions

where ω is the orbital frequency associated with one cpr, a is the amplitude, and θ_0 is the initial phase. The error of along-track SSG due to one cpr error is then

$$\varepsilon_p = \frac{\partial \Delta r}{\partial s} = \frac{\partial \Delta r}{\partial t}\frac{\partial t}{\partial s} = \frac{-a\omega}{v}\sin(\omega t + \theta_0) = a_\varepsilon \sin(\omega t + \theta_0), \quad (10)$$

where v is the satellite's ground speed, which may be calculated by the approximate formula (Hwang and Parsons 1995)

$$\mathrm{v} = \sqrt{\mathrm{v}_x^2 + \mathrm{v}_y^2} = R\sqrt{(\dot{u}\sin\beta - \omega_e'\cos\psi)^2 + (\dot{u}\cos\beta)^2}, \quad (11)$$

where $\dot{u}$ and ω_e' are the velocities of the argument of latitude and the earth's rotation relative to the satellite's orbital plane, respectively, and ψ is the geocentric latitude. Note that practically $\dot{u} = \omega$. The method for computing $\dot{u}$ and ω_e' due to the linear perturbation arising from the earth's flattening can be found in Kaula (1966), and Hwang and Parsons (1995). Using the relationship $\cos i = \sin\beta\cos\psi$, where i is the inclination angle of the satellite's orbital plane, one gets

$$v = R\sqrt{\dot{u}^2 - 2\dot{u}\omega_e'\cos i + \omega_e'^2\cos^2\psi}. \quad (12)$$

Thus we have the maximum ground speed

$$v_{max} = R\sqrt{\dot{u}^2 - 2\dot{u}\omega_e'\cos i + \omega_e'^2}, \text{ if } \psi = 0, \quad (13)$$

and the minimum ground speed

$$v_{min} = R(\dot{u} - \omega_e'\cos i), \text{ if } \psi = i \text{ or } \pi - i. \quad (14)$$

Table 3 lists the estimated amplitudes of one cpr orbit error for all satellite missions, which are based on the assumption that crossover differences with T/P are completely due to the one cpr orbit error (Shum et al. 1990) and T/P orbit errors are negligible. This assumption may not be realistic in the presence of large resonance orbit error. The NSWC orbit of Geosat/GM has a precision of 0.6 m (Cheney et al. 1991). According to Table 3, the ground speed varies very little from its minimum to its maximum, so the amplitudes of along-track SSG error due to one cpr orbit error are practically constant. Except for Seasat and Geosat/GM, the errors in along-track SSG induced by the one cpr orbit error are negligible compared to the instrument noises. Furthermore, the one cpr error is mostly caused by the errors in the gravity field and the initial state vectors for the orbit integration (Engelis 1987), thus its amplitude and the initial phase vary from one satellite revolution to another. Nevertheless, by using the model of (9) for orbit error in the global crossover adjustment of SSH (Rummel 1993), in theory the amplitudes and the initial phases can be estimated. A local adjustment of SSH using a bias-only model will not produce any difference for along-track SSG since the bias in a satellite arc is automatically removed upon differentiation of SSH. Also, if the one cpr error is indeed the dominant orbit error, then the effect of other orbit error components on SSG may be neglected because the effect of one cpr error is already small.

Table 3. The amplitudes of errors in sea surface height and along-track sea surface gradient induced by one cpr orbit error

Satellite mission	a (m)	v_{max} (km s^{-1})	v_{min} (km s^{-1})	$\lvert a_\varepsilon \rvert$ (μrad)
Seasat	0.75	6.788	6.773	0.115
Geosat/ERM	0.35	6.788	6.773	0.054
Geosat/GM[a]	0.60	6.788	6.773	0.092
ERS-1/35d	0.23	6.697	6.681	0.036
ERS-1/GM	0.44	6.697	6.681	0.068
T/P	0.04	5.760	5.744	0.006

[a] Estimate

Ocean tide model induced error

Another error effecting SSH and in turn SSG is the error in the ocean tide model used for correcting the instantaneous SSH. Recent global ocean tide models, largely based on satellite altimetry, are able to achieve very high accuracy. For example, the comparison made by Andersen et al. (1995) shows that the tides M_2, S_2, K_1, and O_1 derived from two years of T/P data have rms discrepancies of less than 2 cm with the measurements at selected tide gauge stations, which are mostly located in the open oceans. However, if such a comparison is restricted to shallow waters or area with large bathymetric features where the spatial variation of ocean tides are much larger than those in the open oceans (Cartwright 1993), the discrepancies increase substantially. The reason for the difference in rms discrepancy is partly numerical: smooth functions such as ocean tides in the open oceans are easier to model than "rough" functions such as ocean tides over shallow waters or area with large bathymetric features. This numerical difference also implies that SSH in the open oceans are less contaminated by ocean tide model error than over shallow waters. Furthermore, if the tide model error consists largely of long wavelength components (see Ma et al. 1994) as does the one cpr orbit error, it will have a much smaller effect on SSG than on SSH.

Table 4 shows a comparison for the M_2tide over 1993–1994 between the tide gauge measurements and the CSR3.0 tide model, which was developed at the Center for Space Research, University of Texas at Austin, based on two years of T/P data. The geographical locations of the used tide gauge stations, which are not included in the "standard" tide gauge set used by Andersen et al. (1995), is shown in Figure 2. In general, the rms discrepancies at all stations are much larger than 2 cm. Along coastal areas, the rms discrepancies fluctuate rapidly. The 5.6 cm discrepancy at Yap, located at the deep ocean, is still considered large. The rms discrepancies over the Ryukyu islands, which are

Table 4. Root-mean-squared discrepancy in M_2 tide between tide gauge measurements and the tide values computed from CSR3.0 ocean tide model over 1993–1994

ID[a]	Station name	Rms discrepancy (cm)
1	Keelung	21.1
2	Anping	7.9
3	Sukangzu	10.1
4	Fukang	4.3
5	Penghu	13.1
6	Yap	5.6
7	Malakal	14.9
8	Quarry Bay	18.4
9	Aburatsu	5.1
10	Kota Kinabalu	7.1
11	Xiamen	28.8
12	Kushimoto	10.0
13	Maisaka	12.2
14	Mera	2.27
15	Naha	13.6
16	Naze	11.5

[a] See Figure 2

surrounded by complex bottom topography, are also large. If the CSR3.0 tide model is to be used in future's generations of altimeter data, then users from China, Japan, Taiwan, and other countries in the South East Asia should be aware of the size of tide model error in the altimeter data.

If repeat measurements of SSH are available at the same location, the tide model induced error will be reduced in the averaged SSH according to a theory below. Neglecting the orbit error and the astronomical argument, an altimeter measured SSH at epoch t_k corrected with the ith tidal component of tide model may be expressed as

$$SSH_k = h_0 + U_i(\phi, \lambda)\cos(\omega_i t_k) + V_i(\phi, \lambda)\sin(\omega_i t_k) \ , \tag{15}$$

where h_0 is the true SSH, U_i and V_i are the quantities that can be sued to calculate the errors of tide in amplitude and phase, and ω_i is the tidal frequency. Assuming that we have M consecutive measurements, the average is

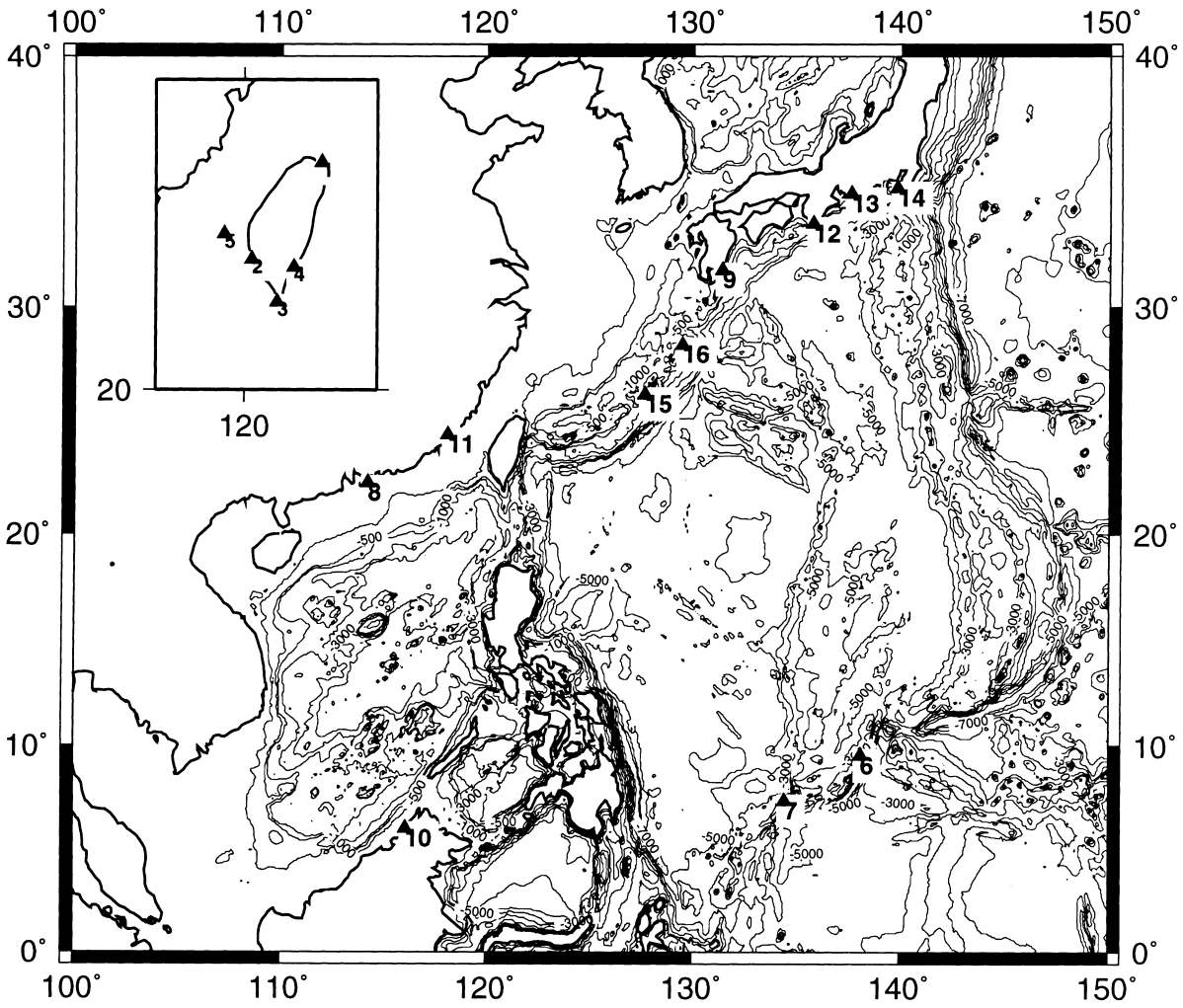

Fig. 2. Distribution of tide gauge stations where the CSR3.0 tide model is compared. Inserted map shows the stations over Taiwan

$$\overline{SSH} = \frac{1}{M}\sum_{k=0}^{M-1} SSH_k = h_0 + \frac{1}{M}U_i(\phi,\lambda)\sum_{k=0}^{M-1}\cos\,(\omega_i t_k) + \frac{1}{M}V_i(\phi,\lambda)\sum_{k=0}^{M-1}\sin\,(\omega_i t_k) = h_0 + \Delta U_i + \Delta V_i\ . \tag{16}$$

What will be the number M to make U_i and V_i vanish from (16)? To answer this, we let

$$t_k = T + k\ \Delta t,\ \ k = 0,1,2,...,M-1\ , \tag{17}$$

where T is the initial epoch and Δt is the satellite's repeat period. substituting (17) into (16) and evaluating the trigonometric series for U_i and V_i, we get

$$\Delta U_i = \frac{1}{M}U_i\cos\,\left[\omega_i\,(T + \frac{M-1}{2}\Delta t)\right] \sin\,\frac{M\omega_i\Delta t}{2}\csc\frac{\omega_i\Delta t}{2} \tag{18}$$

and

$$\Delta V_i = \frac{1}{M}V_i\sin\,\left[\omega_i(T + \frac{M-1}{2}\Delta t)\right]\sin\,\frac{M\omega_i\Delta t}{2}\csc\frac{\omega_i\Delta t}{2}\ . \tag{19}$$

Thus

$$\overline{SSH} = h_0 + \frac{1}{M}\sqrt{U_i^2 + V_i^2}\cos\,[\omega_i(T + \frac{M-1}{2}\Delta t) - \Psi]. \sin\frac{M\omega_i\Delta t}{2}\csc\frac{\omega_i\Delta t}{2}\ , \tag{20}$$

where $\Psi = \tan^{-1}(V_i/U_i)$ is the phase of the tide model error. Assuming that we have the worst case where $\Psi = \omega_i[T + (M-1)\Delta t/2]$, then

$$\overline{SSH} = h_0 + \frac{1}{M}\sqrt{U_i^2 + V_i^2}\sin\frac{M\omega_i\Delta t}{2}\csc\frac{\omega_i\Delta t}{2}\ . \tag{21}$$

To make the tide model error vanish, we should have

$$\sin\frac{M\omega_i\Delta t}{2} = 0\ , \tag{22}$$

which will require $M\omega_i\Delta t = 2\pi,\ 4\pi,\ldots,$ or $M = 2\pi/(\omega_i\Delta t),\ 4\pi/(\omega_i\Delta t),\ldots$. For example, we have the repeat period $\Delta t = 9.9156$ solar days for T/P and ω_i=1.40519 $\times 10^{-4}$s^{-1} for M_2 tide, thus M=0.052192944k where k is an integer. Therefore there is no such k value that will make M an exact integer, namely, we cannot make the tide model error exactly zero by averaging. However, we can always find an integer M such that the tide model error is minimum under some condition (for example, M must be such that the time for averaging the SSH does not exceed 3 years). Note that the tide model error is averaged SSH is governed by the periodic term $\sin M\omega_i\Delta t/2$ and the damping factor 1/M. Assuming that the error of M_2 in amplitude ($\sqrt{U_i^2 + V_i^2}$) is 10 cm we list in Table 5 the errors in averaged SSH due to M_2 error over various averaging periods. A special note will be given to the S_2 error in ERS-1/35d. With $\Delta t = 35$ solar days for ERS-1/35d and $\omega_i = 1.45444 \times 10^{-4}$s^{-1} for S_2 the value $\omega_i\Delta t/2$, after subtracting the integral multiple of 2π, is very close to zero, so the product 1/M $\sin(M\omega_i\Delta t/2)\csc(\omega_i\Delta t/2)$ is nearly 1 for any M, and the magnitude of S_2 error remains unchanged after averaging. In other words, for the sun-synchronous ERS-1/35d mission averaging SSH cannot reduce the S_2 error.

Table 5. Errors (in cm) in averaged sea surface heights due to 10 cm error in M_2 tide for various averaging periods

Averaging period	Geosat/ERM	ERS-1/35d	T/P
3 months	3.02	1.24	2.26
6 months	1.73	1.17	0.12
1 year	0.55	0.87	0.41
2 year	0.50	0.52	0.25
3 year	0.28	0.35	0.18

This analysis has neglected the fact that one cannot always get consecutive SSH values from repeat cycles that are needed to evaluate the trigonometric series in (16). Also, altimeter observations do not repeat the exact location. The second problem is less critical because within a short distance (~ 1 km) the ocean tide is not expected to vary substantially. The first problem is critical near shallow waters, because data there are often edited out due to criteria such as significant wave height (SWH) and ocean tide. In conclusion, theoretically an almost ocean tide-error free sea surface may be formed by averaging a sufficiently long record of SSH if we do not have the unfortunate match of a tidal frequency and the repeat period as in the case of ERS-1/35d. Thus the tide model induced error in along-track SSG derived from averaged SSH is automatically reduced. However, for Seasat, Geosat/GM and ERS-1/GM missions which do not have repeat measurements, the short wavelength tide model error will have a significant impact on along-track SSG. This can only be resolved by an accurate ocean tide model, or, less promisingly by modeling the covariance function of the tide error as below.

The effect of sea surface topography

The sea surface topography (SST) may be decomposed into the quasi-stationary component and the time-varying component, the former being nearly stationary in position and magnitude over a long period of time (e.g., years), the latter evolving rapidly. If one assumes that SSG is identical to geoid gradient, an error will be introduced by the SST and now we wish to see the magnitude of the error. Along the path of an energetic current such as the Kuroshio Current and the Gulf Stream, the SST will create a large slope perpendicular to the path. For example, Hwang (1996) found that the yearly mean slope due to the Kuroshio Current east of Taiwan is 63cm/120km (5.25 μrad); south of Japan the

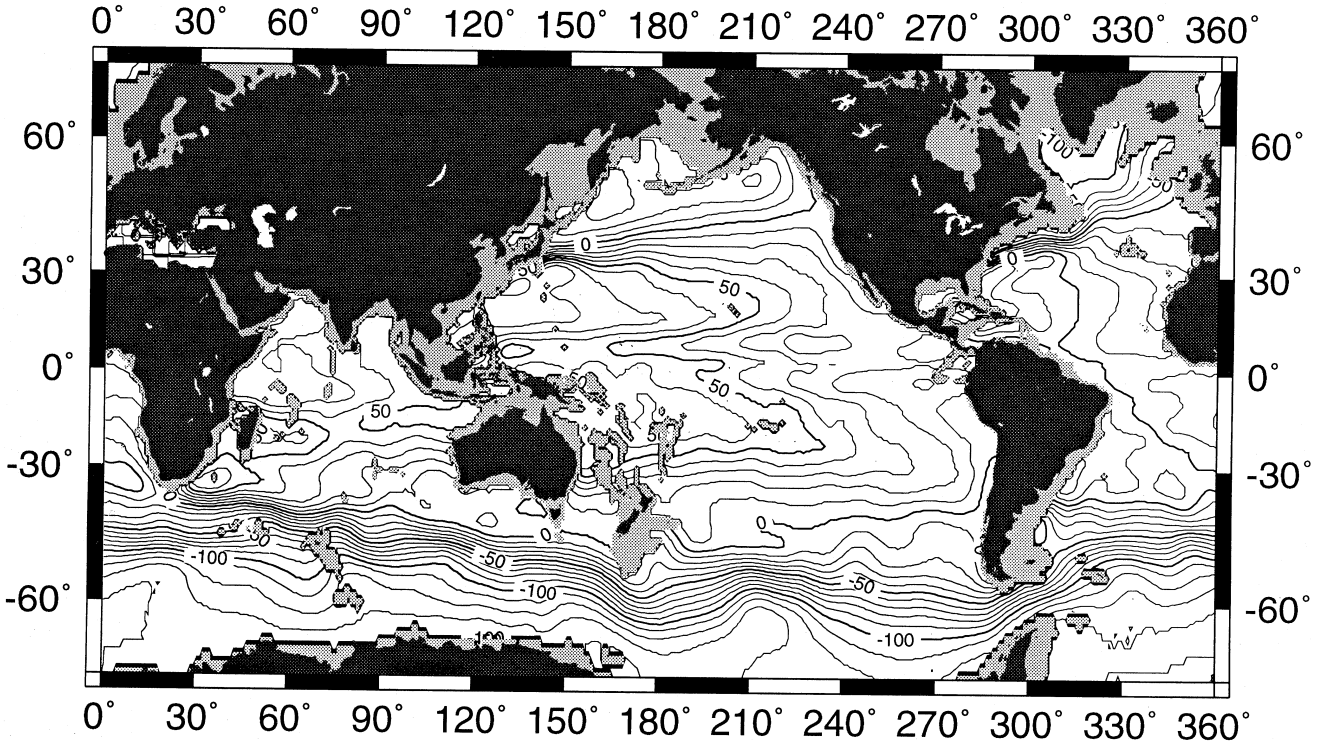

Fig. 3. Quasi-stationary sea surface topography compiled by Levitus, contour interval is 10 cm and areas without data are masked with light gray

largest yearly mean slope due to the Kuroshio Current is 113cm/132km (8.56 μrad). Since the mean percentage variability of the Kuroshio Current is 25% (Hwang 1996), the error can not be removed by averaging as in the case of ocean tide model error. Figure 3 shows the 70-year averaged SST compiled by Levitus (1982). Unfortunately, the SST values are not available near shallow seas, e.g., the East China Sea, the continental shelf of Europe, the east coast of USA, and the coastal area of Australia, thus the Levitus SST is not useful for removing the SST effect there. Also, the Levitus SST contains only signal components with wavelengths longer than 800 km due to data smoothing, so steep slopes such as those crossing the fronts of the Kuroshio and the Gulf Stream can not be derived from the data. Similar problems exist in altimeter-derived low-degree SST models. Nevertheless, the Levitus SST is useful in reducing the SST effect in the open oceans. As an example, Figure 4 shows the absolute gradients of the Levitus SST. The assumption of 2000-db level of no motion in the Levitus SST will not affect the gradients because the DC bias will be eliminated upon differentiation. Using the rule of thumb that 1-μrad error in geoid gradient will translate into 1-mgal error in gravity anomaly one can easily estimate the error due to neglecting the quasi-stationary SST. Indeed, at the areas of major currents, the effects of the quasi-stationary SST are too large to neglect. Also, Table 6, based on Stewart's estimate (Stewart 1985), shows the typical magnitudes of sea surface slopes relative to the geoid created by some ocean phenomena that cause the deviation of the sea surface from the marine geoid. Of these ocean phenomena, the Equatorial Currents can be safely neglected due to the relatively small slopes and the 100% variability when considering the current altimeter data accuracies; The Eastern Boundary Currents, mesoscale eddies and rings have 100% variabilities and hence their effects may be reduced by averaging, but will introduce significant effects for data from the non-repeat Seasat/Geosat/GM and ERS-1/GM. For example, it is well-known that over the Gulf Stream area and the Kuroshio Extension, cold and warm rings exist due to the meandering of these powerful currents. The time-varying SST may be removed if a forecasting model is available e.g., the model of Glenn et al. (1987) provides weekly predictions of the Gulf Stream and ring positions.

Summary and recommendations

- Non-geocentricity induced error: only Seasat needs this correction and the correction is $-0.129\cos\phi\sin\alpha$.
- One cpr error: only Seasat and Geosat/GM need this correction; Do not attempt a bias-only crossover adjustment of SSH because it does not make any difference for SSG.
- Tide model induced error: For averaged Geosat/ERM, ERS-1/35 and T/P this correction is not necessary if there are no data gaps in averaging. For Seasat, ERS-1/GM and Geosat/GM this correction may not be necessary in the open oceans; over shallow water (less than 100 m in depth) replace the global tide model used in the altimeter data by a local

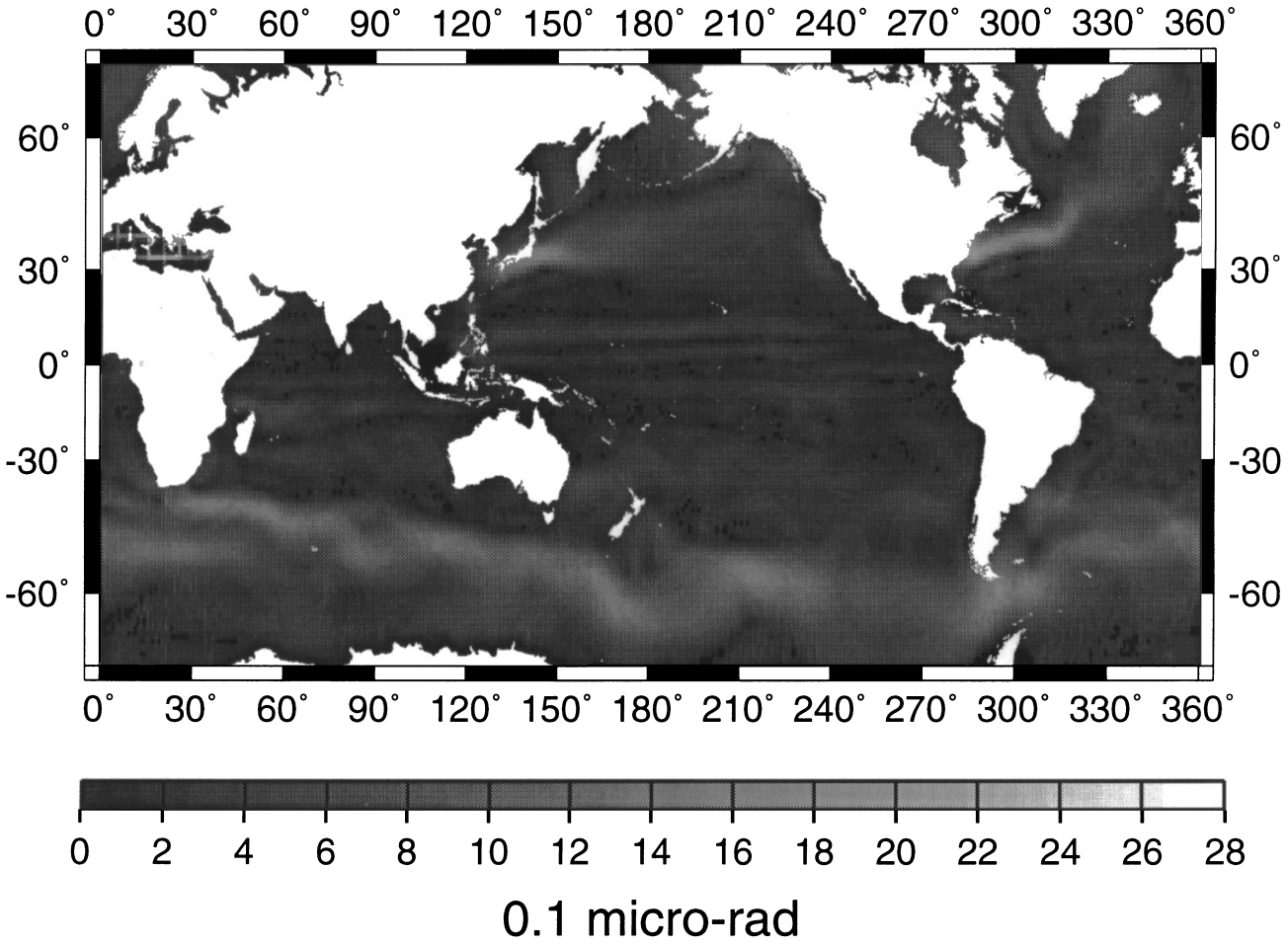

Fig. 4. The absolute slope of the Levitus sea surface topography relative to the geoid

tide model constructed using local tide gauge measurements.

- SST effect: to make the assumption SSG = geoid gradient valid try to remove the quasi-stationary SST from all data and, in addition, try to remove the time-varying SST using a forecasting model for Seasat, ERS-1/GM and Geosat/GM data.

Seasat and Geosat/ERM now have new orbits based on the most up-to-dated tracking networks and force models, see Haines et al. (1994) for Seasat, and Williamson and Nerem (1994) for Geosat/ERM. With the new orbits the errors due to non-geocentricity and one cpr orbit error in SSG for Seasat and Geosat/ERM are almost negligible. One can predict that a global ocean tide model solely based on altimeter data will probably never satisfy the required accuracy over shallow waters (see Table 4 as an example) unless tide gauge measurements are used for modeling. In addition to the three errors discussed above, errors arising from ionospheric corrections, wet/dry tropospheric corrections, time tag correction, significant wave height, clouds/rain, earth tide, instruments bias, etc., will also affect SSH and in turn SSG. Some of these errors are functions of both space and time and are difficult to characterize. Any error that contains mostly long

Table 6. Typical sea surface topography and slope based on Stewart's estimate

Phenomennon	Typical slope relative to geoid (μrad)	Percentage variability in position (%)	Period of variability
Western Boundary Currents	13.00 (130cm/100km)	25	days to years
Large gyre	0.17 (50cm/3000km)	25	one to many years
Eastern Boundary Currents	3.00 (30cm/100km)	100	days to years
Mesoscale eddies	2.50 (25cm/100km)	100	100 days
Rings	10.00 (100cm/100km)	100	weeks to years
Equatorial Currents	0.06 (30cm/5000km)	100	months to years

wavelength components will introduce less trouble for SSG than for SSH.

If LSC is used as the prediction technique, we can account for these errors in SSG by including the covariance functions pertaining to individual errors, in analogy to the method used by Knudsen (1991). To do this we can model the covariance function of an error affecting SSH between points P and Q as

$$C_x(t) \sum_{n=0}^{\infty} \sigma_n^x P_n(t) \ , \tag{23}$$

Where "x" stands for the error to be modeled, σ_n^x is the degree variance of the error, and $P_n(t)$ is the Legendre polynomial of degree n. The variable t is a function of both space and time in that

$$t = \cos(\psi + k^x|\tau_i - \tau_j|) \ , \tag{24}$$

where ψ is the spherical distance between P and Q, τ_i and τ_j are the epochs when the observations are made at P and Q, respectively, and k^x is a conversion factor from time to spherical distance. Suggested models of σ_n^x and k^x may be found in Knudsen (1991). Then, using the law of covariance propagation (Moritz 1980), we can get the covariance function between an error gradient at P with azimuth α_P and an error gradient at Q with azimuth α_Q by (Hwang 1996)

$$\begin{aligned} C_{x'}(t, \alpha_P, \alpha_Q) =& C_{ll}^x(t) \cos(\alpha_P - \alpha_{PQ}) \cos(\alpha_Q - \alpha_{PQ}) \\ &+ C_{mm}^x(t) \sin(\alpha_P - \alpha_{PQ}) \sin(\alpha_Q - \alpha_{PQ}) \ , \end{aligned} \tag{25}$$

where α_{PQ} is the azimuth from P to Q, and C_{ll}^x and C_{mm}^x are the covariance functions of the longitudinal and transverse components of the gradient of the error which are isotropic and are dependent on t only. See also Hwang (1996) for the method of computing C_{ll}^x and C_{mm}^x given σ_n^x.

Geoid determination over Taiwan using gravity anomalies and altimeter-derived sea surface gradients

The gravity data and corrections for systematic errors

The gravity data to be used are the land gravity anomalies collected by Yen et al. (1990) over Taiwan and the ship gravity anomalies from the National Geophysical Data Center. The land gravity anomalies are based on the GRS67 system and the rigorous free-air reduction formula. The long-track sampling rates of the reduction formula. The along-track sampling rates of the ship data vary from one cruise to another. To make the density of the ship gravity compatible with the density of the land gravity, and to reduce the computational time, for each $3' \times 3'$ bin with a least one data point we select the ship gravity anomaly which has the median value. Also, the ship gravity anomalies were adjusted to remove biases and trends using a satellite-only gravity anomaly field (Hwang and Parsons, 1995). The distribution of the land data and the selected ship data is shown in Figure 5. To be consistent with the 5 μgal instrument accuracy, we apply the following corrections to the land gravity anomalies, according to the analysis by Heck (1990):

- Correction to GRS80 system (Torge, 1989)

$$\Delta g_1 = -0.90 - 0.0045 \sin^2 \phi \ \text{(mgal)} \tag{26}$$

- Atmoshpheric correction

$$\Delta g_2 = 0.87 \ \text{mgal}$$

- Correction for vertical datum inconsistency (Heck, 1990, Table 1)

$$\Delta g_3 = -0.09 \ \text{mgal}$$

- Correction for horizontal datum inconsistency

$$\Delta g_4 = 0.0251 \sin 2\phi \delta\phi \ \text{(mgal)} \ , \tag{27}$$

where $\delta\phi$ is measured in arc-second and can be calculated by

$$\begin{aligned} \delta\phi = & -\frac{e^2}{2} \sin 2\phi \ \delta m - (\sin\lambda \alpha_x - \cos\lambda \alpha_y) \\ & - \sin\phi \cos\lambda \frac{T_x}{a} - \sin\phi \sin\lambda \frac{T_y}{a} + \cos\phi \frac{T_z}{a} \\ & + \frac{e^2}{2} \sin 2\phi \frac{\delta a}{a} + \sin 2\phi \delta f \ , \end{aligned} \tag{28}$$

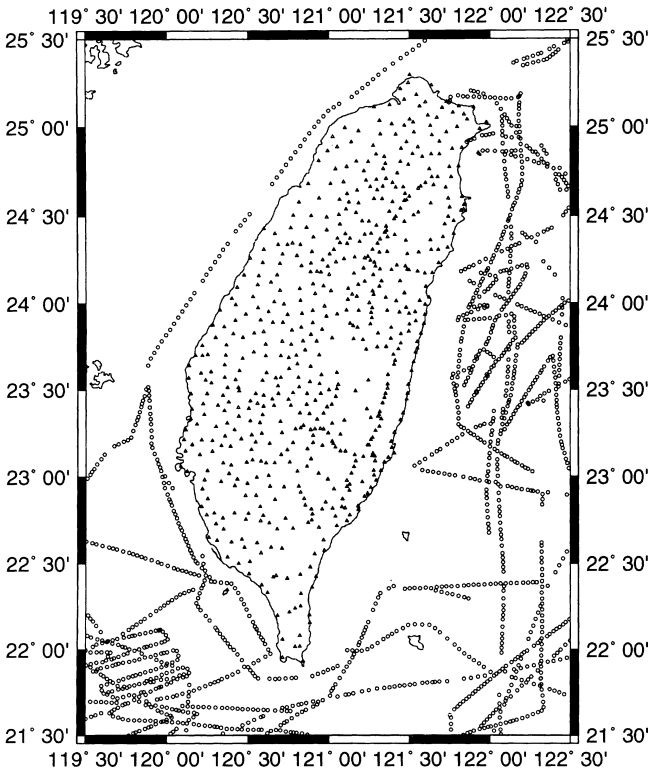

Fig. 5. Distribution of land gravity anomalies over Taiwan (triangle) and ship gravity anomalies (circle) used for the geoid determination

where the needed 7 transformation parameters from Taiwan's geodetic system to the WGS84 system, which is assumed to be geocentric, are obtained from Chen et al. (1993):
Scaling factor $\delta m = 23.142 \times 10^{-6}$;

Translations $T_x = -751.637$ m, $T_y = -358.568$ m,
$T_z = -179.421$ m;

Rotations $\alpha_x = -0.373''$, $\alpha_y = 0.686''$, $\alpha_z = 0.291''$.
The change in ellipsoidal parameters is:

$\delta a = 6378137 - 6378160 = -23$ m;

$\delta f = 0$.

The values Δg_4 range from -0.115 to -0.126 mgal.
These corrections are to be added to the gravity anomalies provided by Yen et al. (1990). The magnitude of the total correction is about -0.240 mgal islandwide. Furthermore, to be consistent with the coordinate systems of the altimeter data and the ship data, the geodetic coordinates of the gravity data points based on Taiwan's geodetic datum are converted to the coordinates in the WGS84 system using the 7 transformation parameters listed above. For this conversion the change in latitude can be calculated by (28) and the change in longitude by (Rapp 1989)

$$\delta\lambda = \alpha_x \tan\phi \cos\lambda + \alpha_y \tan\ \phi\ \sin\lambda - \alpha_z - \frac{1}{a\cos\phi}(T_x \sin\lambda - T_y \cos\lambda)\ . \tag{29}$$

The changes due to the datum conversion range from $-6.60''$ to $-6.21''$ in latitude, and from $28.92''$ to $29.70''$ in longitude. The contour map of the corrected land gravity anomalies and the selected ship gravity anomalies is shown in Figure 6. The maximum and minimum values are 327.515 (on land) and -238.418 (at sea) mgals, respectively, and the standard deviations on land and at sea are 93.155 and 62.304 mgals, respectively. The gravity map features highs along the Central Range of Taiwan and lows offshore east coast of Taiwan where a deep trench exists. Over the west coast of Taiwan the gravity anomalies are negative due to sediments.

The altimeter data

Because only few ship cruises are available, the ship data are rather sparse and are not sufficient to fill the data gap offshore Taiwan. Thus using the gravity data alone the coastal geoid may be poorly determined. Altimeter data just add to the ship data at sea. Based on the analysis above, along-track SSG contains less systematic errors than SSH, especially when the systematic errors in the original SSH contain largely long wavelength components. Thus SSG will be the data type to be used. Since SSG are only available at sea, they are located at the "remote" zone when determining the land geoid. Again, to reduce the computational time for a $3' \times 3'$ non-empty bin we select only the along-track SSG with the smallest error. Figure 7 shows the distribution of the "binned"

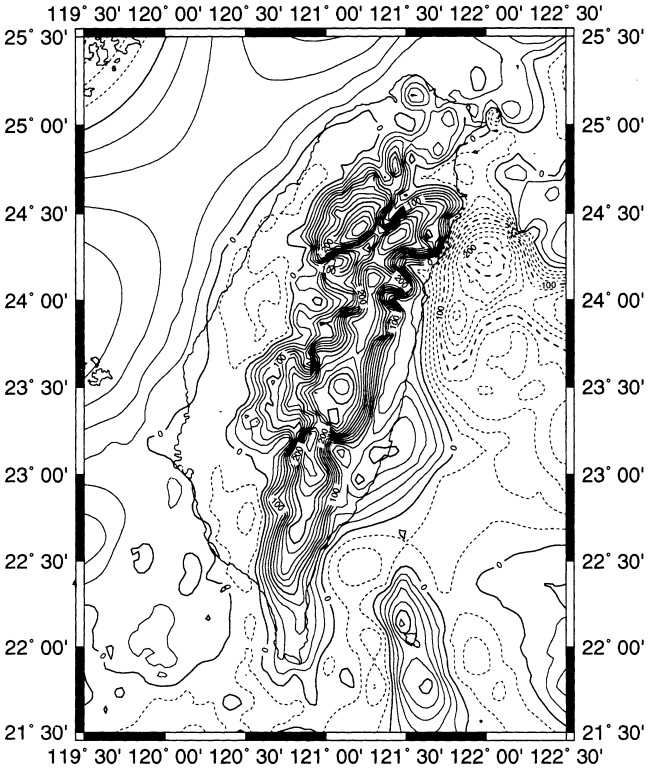

Fig. 6. Gravity anomalies over Taiwan (see Figure 5 for data distribution), contour interval is 20 mgals. The solid contours indicate positive values, while the dashed contours indicate negative values

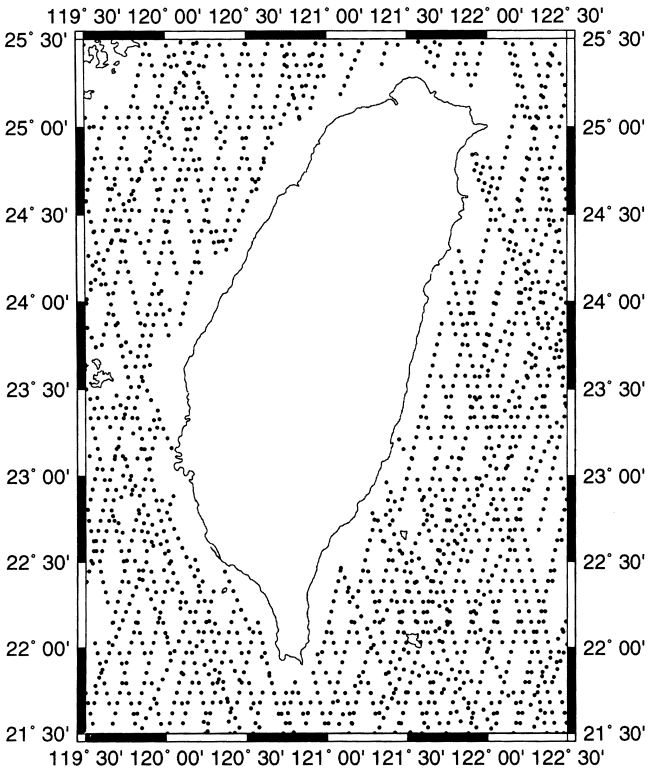

Fig. 7. Distribution of the binned $3' \times 3'$ sea surface gradients derived from Seasat, Geosat/ERM, ERS-1/35d, ERS-1/GM and TOPEX/POSEIDON altimeter data

SSG around Taiwan. The Geosat/GM data were not available at the time of writing this paper. The densest data come from ERS-1/GM, while T/P contributes the least. Of the phenomena listed in Table 6, only the Kuroshio Current is known to exist within 50 km to the shore of east Taiwan and its effect will be modeled in LSC (see below). According to Table 4, possible tide model errors exist in all altimeter data due to the complete bathymetry and shallow waters, especially for the non repeat Seasat and ERS-1/GM. However, it is beyond the scope of this study to model the ocean tide error and other errors. By evaluating the quality of the predicted geoid we will see whether the errors have seriously affected the altimeter data.

The elevation data and residual terrain model for a mixed land-sea area

It is estimated that the averaged data spacing of the land gravity anomalies over Taiwan is 2′ to 3′. To obtain a local geoid with resolution higher than that of gravity data we have to rely on elevation data (Forsberg 1984). In this study, the digital terrain model (DTM) on Taiwan is provided by Shih (1995). Shih's DTM is based on the Digital Chart of the World published by the Defense Mapping Agency of USA and is on a $30'' \times 30''$ grid.Because RTM reductions are also needed at sea for the ship and altimeter data, we also used the bathymetry data from ETOPO5. To avoid discontinuity along coastal areas, the $30'' \times 30''$ DTM grid and the $5' \times 5'$ ETOPO5 grid were first transformed to point data with positive elevations from DTM only and depths from ETOPO5 only. Then, a new $30'' \times 30''$ grid was created from the point data by a minimum curvature interpolation scheme. Comparisons show that on land the new $30'' \times 30''$ grid is almost identical to the old one with differences on the order of few meters, and at sea the new grid and the ETOPO5 grid agree well but a the trench the differences can be up to 50 m. Figure 8 shows the combined DTM-ETOPO5 model, which has a standard deviation of 1825 m. The mean and the standard deviation of the DTM are 783 m, and 827 m, respectively, with a peak of 4000-m high at the center. At the populated east coastal area, mountains of 2000-m high are only about 10 km away from the sea shores. Then, less than 50 km offshore the northeast coast of Taiwan where the Philippine Sea plate meets the Eurasian plate, the subducting Philippine Sea plate creates a 5000-m deep trench. Over the west coast the change of terrain is relatively smooth, but in the northern part of the island the change is equally large as the east coast.

The elevation data can be used to compute the effects on the functionals of the earth's gravity field due to the mass layer between the actual topography and a reference topography, the so-called RTM effects. In this study the required RTM effects are for gravity anomalies, geoid gradients and geoid undulations. The RTM effects are removed from the raw data to produce the relatively smooth residual data, which are then used for geoid the computation. The complete list of the formulae for RTM computations using FFT can be found in Schwarz et al. (1990). RTM effects are either evaluated solely on land, e.g., Forsberg (1984), or solely at sea e.g., Basic and Rapp (1992). For the computations over a mixed land-sea domain the formulae suitable for the FFT technique must be modified. The modification is associated with the use of densities of the sources that generate the RTM effects over land and ocean. Assuming that on land the rock density, ρ_1, is uniformly 2.67 g/cm^3, and at sea the density difference between rock and sea water, ρ_2, is also uniformly 1.64 g/cm^3, the linear terms of RTM effects can be computed as follows.

•RTM effect on geoid

Considering the density is a function of position, the effect is:

$$N_{RTM}(x_p, y_p) = \frac{G}{\gamma}\int_E \frac{\rho(x,y)(h(x,y) - h_r(x,y))}{\sqrt{(x-x_p)^2 + (y-y_p)^2}}\,dxdy$$
$$= \frac{G}{\gamma}\left[\rho(h-h_r)\right] * \frac{1}{r} = \frac{G}{\gamma}\rho_1\left[(\overline{h} - \overline{h}_r) * \frac{1}{r}\right] , \tag{30}$$

where $''*''$ is the convolution operator, E is the domain of integration in the X-Y plane, γ is the normal gravity, $r = \sqrt{x^2 + y^2}$, h and h_r are the actual elevation and the reference elevation, respectively, and

$$(\overline{h}, \overline{h}_r) = \begin{cases} (h, h_r), \text{ if land} \\ \rho_2/\rho_1(h, h_r), \text{ if ocean} \end{cases} \tag{31}$$

which are the scaled elevations (note: at sea the elevation is negative). By Fourier transforming (30), the spectrum of N_{RTM} is the product of the spectrum of the scaled elevations and the spectrum of 1/r (subject to a constant factor). This then enables a fast computation of N_{RTM}. Likewise we may get the following RTM effects.

•RTM effect on gravity

$$\Delta g_{RTM}(x_p, y_p) = 2\pi G\rho_1(\overline{h} - \overline{h}_r) - c(x_p, y_p) , \tag{32}$$

where c is calculated as

$$c(x_p, y_p) = \frac{1}{2}G\rho_1[\hat{h}^2 * \frac{1}{r^3} - 2\hat{h}_p(\hat{h} * \frac{1}{r^3}) + \hat{h}^2{}_p F] , \tag{33}$$

where

$$(\hat{h}, \hat{h}_p) = \begin{cases} (h, h_p), \text{ if land} \\ \sqrt{\rho_2/\rho_1}(h, h_p), \text{ if ocean} \end{cases} \tag{34}$$

and

$$F = \int_E \frac{1}{r^3}\,dxdy . \tag{35}$$

On land the term in (33) is called terrain correction, whereas over ocean it is simply a correction to the effect of Bouguer plate enclosed by the actual depth and the reference depth.

• RTM effect on deflection of the vertical

$$\begin{pmatrix} c_\xi \\ c_\eta \end{pmatrix} = -\frac{G\rho_1}{\gamma}\left[(\overline{h} - \overline{h}_r) * \begin{pmatrix} y/r^3 \\ x/r^3 \end{pmatrix}\right] , \tag{36}$$

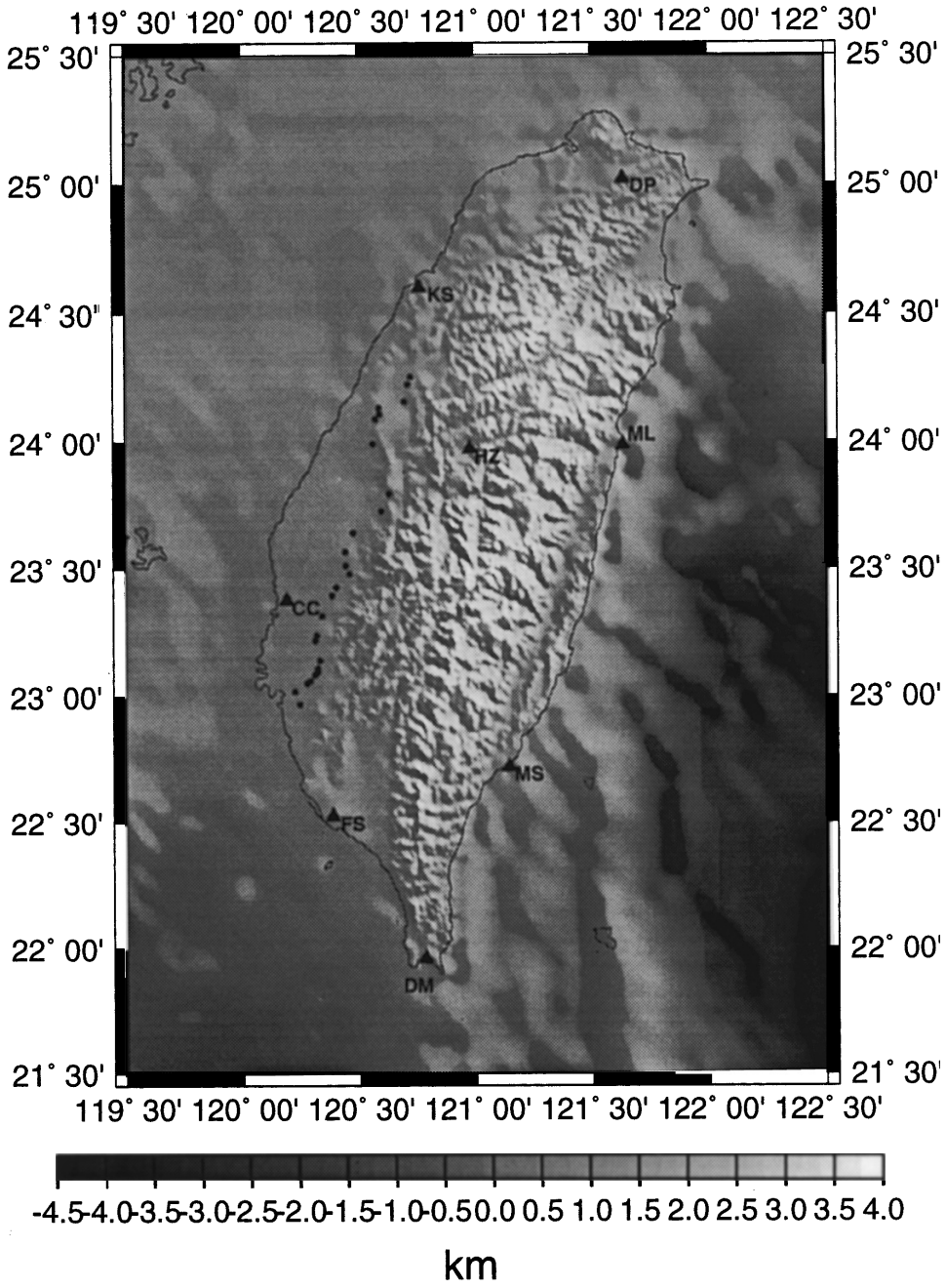

Fig. 8. Gray-shaded map of the combined DTM-ETOPO5 elevation model with illumination from the Northeast, also plotted are the distributions of the 26 benchmarks (solid circle) and 8 astrogeodetic stations (solid triangle and with the initial of the station name) for geoid comparison

where C_ξ, C_η are the north and east components of deflections of the vertical, respectively. Note that geoid gradient and deflection of the vertical bear opposite sign. Also, equations (30), (33) and (36) represent only the first order approximations of the RTM effects. The actual computations were carried out using program "tcfour" developed by Forsberg (1984) with modifications for the mixed land-sea domain. The reference elevations were generated from the new $30'' \times 30''$ elevation grid using a median filter with a filter length of 50 km. The spectra of the kernel functions $1/r$, l/r^3, x/r^3, y/r^3 are computed discretely by FFT. Table 7 shows the statistics of the RTM effects over the area $121°.5 < \text{longitude} < 122°.5, 21°.5 < \text{latitude} < 25°.5$.

Geoid determination by least-squares collocation

Since SSG is heterogeneous to gravity anomaly, we have to use least-squares collocation (LSC) for the geoid determination when using both SSG and gravity anomalies simultaneously. With a remove/restore procedure, the residual geoid undulation is computed as

Table 7. RTM effects over 121°<longitude<122°.5, 21°.5 <latitude<25°.5 using a combined DTM-ETOPO5 model and a 30′ × 30′ reference elevation model

	Gravity anomaly (mgal)	Geoidal height (m)	Deflection north (arc-sec)	Deflection east (arc-sec)
Maximum	163.8	1.53	20.28	21.19
Minimum	−176.4	−0.72	−21.31	−22.16
Mean	−0.1	0.15	0.01	0.01
Std. dev.	21.7	0.34	2.73	3.29

$$N_{res} = (C_{N\Delta g} C_{Ne}) \begin{pmatrix} C_{\Delta g} + D_{\Delta g} & C_{\Delta ge} \\ C_{e\Delta g} & C_e + D_e \end{pmatrix}^{-1} \cdot \qquad (37)$$

$$\begin{pmatrix} \Delta g_{res} \\ e_{res} \end{pmatrix},$$

where

$$\Delta g_{res} = \Delta g - \Delta g_{osu91a} - \Delta g_{RTM} \ , \qquad (38)$$

and

$$e_{res} = e - \varepsilon_{osu91a} - \varepsilon_{RTM} = \theta + \varepsilon - \varepsilon_{ousu91a} - \varepsilon_{RTM} \ , \qquad (39)$$

are the residual gravity anomaly and the residual SSG, respectively, with the contributions from OSU91A (Rapp et al. 1991) to degree 360 and the RTM effects removed. The SSG e is the sum of geoid gradient ε and SST gradient θ. The full geoidal undulation is obtained by adding back the contributions from OSU91A and the RTM geoid effect:

$$N = N_{res} + N_{osu91a} + N_{RTM} \ . \qquad (40)$$

In (37) $C_{N\Delta g}, C_{Ne}, C_{\Delta g}, C_{\Delta ge}$, and C_e are covariance matrices for geoid-gravity anomaly, geoid-SSG, gravity anomaly-gravity anomaly, gravity anomaly-SSG, and SSG-SSG, respectively (note: all referring to the residual quantities). Matrices $D_{\Delta g}$, and D_e are diagonal and contain the variances of random noises of the used gravity anomalies and geoid gradients, respectively. In this study, the random noise is 1 mgal for all the land gravity anomalies, considering the uncertainties in the vertical datum and the gravity datum of Taiwan. The noise of the ship data is uniformly 4.21 mgal, based on the estimate by Hwang and Parsons (1995). The noises of SSG vary from one mission to another and they are calculated while averaging repeat cycles, or in the case of non-repeat data we used the noise of SSH to estimate the noise of SSG (see Table 1 and its related information). Assuming that SST gradient is uncorrelated with the earth's gravity field, we have $C_{Ne} = C_{N\varepsilon}$, $C_{\Delta ge} = C_{\Delta g\varepsilon}, C_{ee} = C_{\varepsilon\varepsilon} + C_{\theta\theta}$. In this study, the global covariance functions for $N - \Delta g, N - \varepsilon, \Delta g - \varepsilon$ and $\varepsilon - \varepsilon$ were computed using series expansions in Legendre polynomials with the coefficients of the error part (from degree 2 to 360) based on the error degree variances of the OSU91A gravity model, and the coefficients of the signal part (from degree 361 on) based on Model 4 of Tscherning/Rapp anomaly degree variance (Tscherning and Rapp 1974), see also Hwang (1989), Hwang and Parsons (1995) and Hwang (1996). The global covariance function for θ–θ was computed again in Legendre series with the coefficients based on the spherical harmonic expansion of the Levitus SST to degree 50 (Hwang 1996). A LSC computation is made at one single grid point with data selected within a spherical cap centered at the point. Two scaling factors were applied to the global covariance functions to obtain the actual covariance functions for use in (37). One scaling factor is for $C_{N\Delta g}, C_{N\varepsilon}, C_{\Delta g\varepsilon}, C_{\varepsilon\varepsilon}, C_{\Delta g}$, the other is for $C_{\theta\theta}$, see also Hwang (1996, Appendix B). Tests have been made to see the effect of using different cap sizes. Comparing the GPS-derived and the predicted geoidal heights (see below), the best agreement is obtained with 0.5° cap size. In fact, using LSC the prediction is only accurate when data distances are well within the correlation lengths of the covariance functions (Moritz 1980). Thus, with a large cap size some data distances will be larger than the correlation lengths. Table 8 shows the correlation lengths of the covariance functions used in this study. C^{ε}_{ll} and C^{ε}_{mm} are the covariance functions for the longitudinal and transverse components of geoid gradient, while C^{θ}_{ll} and C^{θ}_{mm} are the covariance functions for the longitudinal and transverse components of SST gradient and these four functions are necessary for computing the covariance function of SSG in (39). The correlation lengths for $C_{l\Delta g}$ (longitudinal component of geoid gradient-gravity anomaly) and C_{ln} (longitudinal component of geoid gradient-geoid) are undefined because $C_{l\Delta g}(0) = C_{lN}(0) = 0$. Except for C^{θ}_{ll} and C^{θ}_{mm}, the correlation lengths are below or equal to 0.5°.

Table 8. Variances and correlation lengths of the covariance functions based on OSU91A error degree variance model to degree 360 and Tscherning/Rapp anomaly degree variance model with A=425.28 mgal^2, B=24

	$C_{\Delta g}$	$C_{N\Delta g}$	C^{ε}_{ll}	C^{ε}_{mm}	C^{θ}_{ll}	C^{θ}_{mm}
Variance	831.75 (mgal^2)	11.25 (m mgal)	18.52 (arc-sec^2)	18.52 (arc-sec^2)	0.01 (arc-sec^2)	0.01 (arc-sec^2)
Correlation length(°)	0.10	0.23	0.07	0.15	2.27	4.33

Table 9. Four solutions for Taiwan's geoid

Solution	Data			RTM
	Land gravity anomaly	Ship gravity anomaly	Altimeter SSG	
A	on	on	on	on
B	on	on	off	on
C	on	on	on	off
D	on	on	off	off

The result of geoid determination

Four solutions for Taiwan's geoid have been made using various combinations of options, as summarized in Table 9. The computations were carried out on a CONVEX C3840 supercomputer. The grid size used is $30'' \times 30''$ (same as that of DTM) for Solution A and B, and is $2' \times 2'$ (the limit of the gravity data resolution) for Solutions C and D. Solutions C and D are designed to see whether the RTM reductions are necessary. Also, in Solutions C and D the terrain corrections from the $30'' \times 30''$ DTM (see (33), but setting zero for elevations at sea) were applied to the land gravity anomalies and the computed co-geoid was corrected by the indirect effect $-\pi G\rho h^2/\gamma$ (Wang and Rapp 1990) with h being elevation. To evaluate the four solutions, we first compare the predicted and the GPS-derived geodial heights along a profile of 26 first-order benchmarks located at the coastal area of the west Taiwan (see Figure 8). In the GPS measuring campaign, six dual-frequency Trimble 4000 SST receivers were used simultaneously, and each benchmark occupied by 2 sessions in one day (Tsuei et al. 1933). Also, the precision ephemeris of GPS was used in the coordinates computation. The standard deviation of the 26 GPS-derived geoidal heights is 0.546 m and the range is 1.918 m. The result of the comparison is shown in table 10. The mean differences between the GPS-derived geoid and the four predicted geoids are about 4.6 m, indicating that the GPS-implied datum and the datums associated with the predicted geoids are different. Therefore, only the geodial height differences should be compared and the standard deviation of the differences is the descriptor of the geoid quality. It is clear from Table 10 that Solution A yields the best geoid. Without altimeter data the accuracy of the predicted geoid is degraded by 27%(A vs. B). Comparing the results from Solutions A and C, it is concluded that for the rugged terrain over Taiwan the RTM procedure is better than the procedure with terrain correction. Figure 9 shows the geoid from Solution A. Note that the 4-cm standard deviation from Solution A is to be compared with the 7-cm standard deviation achieved by Tsuei et al (1994).

Table 10. Difference (in meter) between the GPS-derived and the predicted geoidal heights

Model	Maximum	Minimum	Mean	Std. dev.
A	4.757	4.607	4.673	0.040
B	4.835	4.652	4.725	0.055
C	4.536	4.300	4.456	0.067
D	4.580	4.261	4.404	0.081
OSU91A to 360	3.929	3.232	3.575	0.184

Another comparison, which is indirect, was made using the deflections of the vertical at 8 astrogeodetic stations selected from Taiwan's first-order control network (see Figure 8). Station HZ is the origin of Taiwan's geodetic datum. Similar to (3) and (4), the nor and east components of a deflection can be calculated from the predicted geoid N as

$$\xi = -\frac{\partial N}{R\partial\phi}, \eta = -\frac{\partial N}{R\cos\phi\partial\lambda} \ . \tag{41}$$

The differentiations also remove the constant bias (if any) in the predicted geoid. In practice (41) was done with a numerical method in which the gridded geoidal heights were first approximated by quadratic polynomials in a local horizontal coordinate system. With the coefficients found, the derivatives of the approximating polynomials were then evaluated to get the deflections. A recommended program for this purpose is IMSL's QD2DR. To compare the predicted deflections and the observed deflections, the geoid-implied geodetic datum is converted to Taiwan's datum using a three-parameter transformation model (Heiskanen and Moritz 1985, eq.(5-72):

$$\begin{aligned} \xi' &= \xi + a_1 \sin\ \phi\cos\ \lambda + a_2 \sin\phi\sin\lambda + a_3\cos\phi \ , \\ .\eta' &= \eta + a_1\sin\lambda - a_2\cos\lambda \ , \end{aligned} \tag{42}$$

where ξ', η' are the deflections in Taiwan's datum, and ξ, η are the deflections in the geoid-implied datum. Table 11 shows the result of the comparison, which, in terms of the agreements between the measured and the predicted, is the same as the case of comparing geoidal heights. In particular, the improvement due to the altimeter data is 30% (A vs. B). Special attention is given to Station ML, where the geoid experiences a steep west-east slope due to the high mountains on the left and the deep trench on the right and the east component of the deflection is a relatively large 70.94". At this station the east components from Solution A and from the observation match to 0.68", while Solution B yields a 6.16" discrepancy. The above two comparisons show that, although the altimeter-derived SSG around Taiwan are located at shallow waters and may contain errors, they may not be so seriously contaminated by errors and they indeed help to improve the geoid prediction over Taiwan.

In the engineering application of the geoid, an orthometric height difference can be obtained by

$$\Delta H = \Delta h - \Delta N \ , \tag{43}$$

where the ellipsoidal height difference Δh can be obtained from GPS and the geoidal difference ΔN from a geoid model. This is the so-called GPS leveling, which may

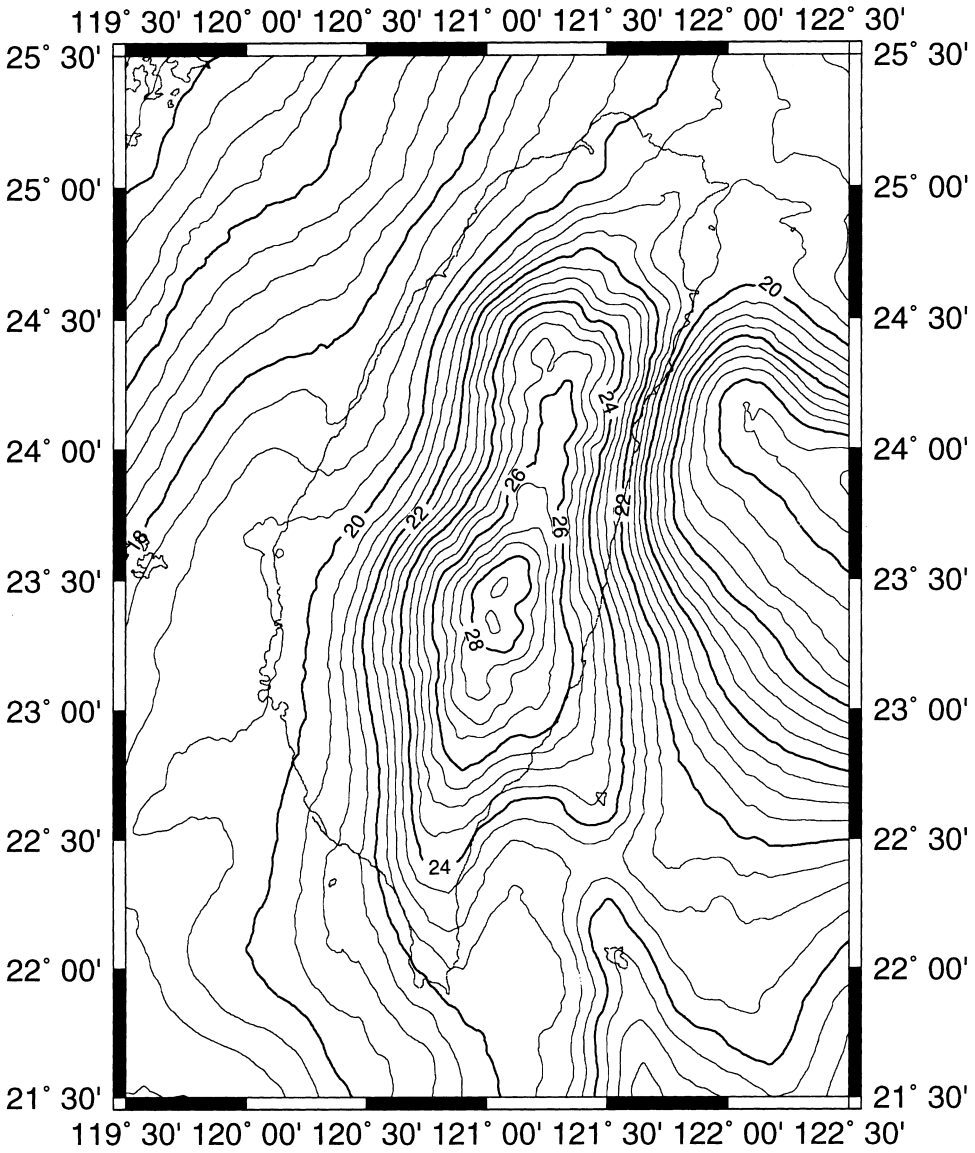

Fig. 9. The predicted geoid over Taiwan from Solution A, contour interval is 0.5 m

replace the conventional leveling. Figure 10 shows the relative accuracies of the orthometric height differences using the geoid model from Solution A along the test profile, as well as the accuracies required in the first second and third-order leveling (Kahmen and Faig 1988 p.385). A relative accuracy between two benchmarks is calculated by $(\Delta H_t - \Delta H_m)$/distance, where ΔH_t is the difference of the two orthometric heights from leveling

Table 11. Comparison of the observed and geoid-derived deflections of the vertical (in arc-second)

Station name	Obs.		Obs. −A		Obs. −B		Obs. −C		Obs. −D		Obs. −OSU	
	ξ	η	ξ	η	ξ	η	ξ	η	ξ	η	ξ	η
DP	−3.23	20.67	−1.84	0.08	−2.51	0.45	2.91	2.14	−1.18	3.69	2.58	−5.99
KS	3.19	13.62	3.68	2.23	3.34	−0.48	2.01	−0.19	3.34	4.48	0.78	5.37
ML	−14.19	70.94	−1.60	−0.68	−0.72	6.16	−4.75	3.37	−3.25	7.00	−7.66	11.02
CC	−6.07	19.30	1.33	1.67	−1.14	0.29	0.11	2.79	0.50	−1.57	−1.82	3.56
MS	−20.16	31.16	0.06	2.97	−4.17	0.81	−1.38	−1.23	−2.77	−1.85	1.37	−0.44
FS	−5.99	17.93	0.21	−1.87	2.83	−2.16	3.15	0.45	4.03	−1.27	8.84	3.27
DM	−14.83	15.68	−0.53	−1.53	3.42	−2.65	1.29	−1.93	2.83	−2.49	−5.74	−6.97
HZ	0.37	−2.07	−1.32	−2.90	−1.08	−2.45	−3.35	−5.42	−3.54	−8.04	1.65	−9.87
Rms	10.73	30.76	1.71	1.98	2.68	2.66	2.73	2.70	2.91	4.48	4.81	6.67

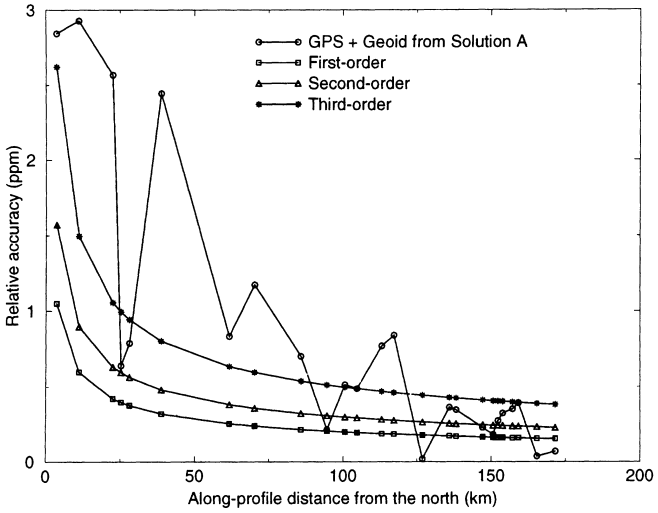

Fig. 10. Relative accuracies of the orthometric height differences derived from GPS ellipsoidal heights and Solution A geoid along the test leveling profile

and ΔH_m is the modeled difference from GPS+geoid. Using the geoid from Solution A the averaged relative accuracy achieved is 0.81 part per million (ppm). In fact, in such a comparison two factors will affect the result. First, the ellipsoidal heights from GPS are not error-free: using the type of Trimble receiver mentioned above, the expected accuracy in ellipsoidal height difference is 10mm+1ppn (see a Trimble user's manual). With 2 sessions of observations and an averaged distance of 85 km, the averaged accuracy for the 25 ellipsoidal height differences is 67 mm. Second, ΔH_t is also subject to a maximum error of $2\sqrt{K}$ mm, where k is the distance in km between two neighboring benchmarks. Using $K = 85$ km the averaged accuracy for ΔH_t is 18 mm. If the error in the ellipsoidal height differences and the error in ΔH_t are only halves of the averaged values, then according to error propagation the projected noise of the geoid from Solution A is 2 cm. Assuming that the error of ellipsoidal height difference from GPS is 5mm+0.5ppm, then a geoid with 2-cm accuracy can help GPS to do the third-order leveling, which demands an error bound of $5\sqrt{K}$ mm.

Discussion and conclusions

In this paper we analyzed the errors of altimeter-derived SSG due to non-geocentricity of satellite reference frame, tide model error and one cpr orbit error. It is found that, in general for the averaged Geosat/ERM, ERS-1/35d and T/P data sets listed in Table 1 these errors are negligible, but for the non-repeat Seasat, Geosat/GM and ERS-1/GM these errors are significant and need to be corrected. If the errors consist mostly of long wavelength components, they will introduce less trouble to SSG than to SSH. If SSH are affected by a constant error, using SSG is equivalent to using crossover adjusted SSH with a bias-only error model, but requires less computational effort than the latter. Based on these considerations it is concluded that SSG is a better data type than SSH. We must point out that all the altimeter data can be updated, and the errors in the new data could be much less severe than the errors contained in the altimeter data sets listed in Table 1. In addition to the previously mentioned works that yielded the new orbits of Seasat and Geosat/ERM, we cite the application of altimetry by Smit and Sandwell (1995) who have replaced the NSWC orbits in Geosat/GM by the T/P compatible JGM-3 orbits, and the Schwiderski tide model by the CSR3.0 tide model. Perhaps the biggest and the most complicated error in satellite altimetry is the ocean tide model error. To support this statement we replaced the Cartwright and Ray tide model in the T/P GDR's by CSR3.0 and found that with CSR3.0 the rms crossover differences over $100^\circ < \text{longitude} < 140^\circ, 0^\circ < \text{latitude} < 40^\circ$ for cycles 2 to 36 are reduced by only 1-2 cm and some crossover differences are still as large as 40 cm.

The altimeter-derived SSG have been successfully incorporated into the geoid prediction over Taiwan. With RTM reductions the inclusion of SSG improve the prediction by 27% when comparing the GPS-derived and the predicted geoidal heights, and by 30% when comparing the observed and the predicted deflections of the vertical. Altimeter data are particularly useful in predicting a precision coastal geoid if there are no marine gravity data at the immediate vicinity of the coastal area. For countries which have dense populations along coastal areas and require a high precision coastal geoid for engineering applications, altimeter data are indispensable.

Acknowledgements. This research was supported by the National Science Council of the Republic of China, under contract NSC84-2211-E-0092-032. The supercomputer resource was provided by the National Center of High performance Computing via this project. I am grateful to R.H. Rapp for providing me the Geosat/ERM data, to H.Y. Yen for the land gravity data, to the Navy of the Republic of China and G. Mitchum for the tide gauge data and to the Center for Space Research, UT Austin, for the CSR3.0 tide model. GMT was used to display the data.

References

Andersen OB, Woodworth PL, Flather RA (1995) Intercomparison of recent ocean tide models – preliminary investigations of recent global ocean tide models with main attention to the Atlantic Ocean and Atlantic shelf regions J. Geophys. Res. 100: 25261–25282.

AVISO (1992) AVISO User Handbook: Merged TOPEX/POSEIDON products, AVI-NT-02-101-CN, edition 2.1.

Basic T, Rapp RH (1992) Oceanwide prediction of gravity anomalies and sea surface heights using Geos-3, Seasat and Geosat altimeter data and ETOPO5U bathymetric data, Rep No. 416, Dept. of Geod. Sci. and Surv., The Ohio State University, Columbus.

Carlowicz M (1995) New map of sea floor mirrors surface EOS, Trans. AGU, 76(44): 441–442.

Cartwright DE (1993) Theory of ocean tides with application to altimetry, in Rummel and Sanso (eds.), Lecture Notes in Earth Sciences, Vol. 50, Springer-Verlag, New York, pp.99–141.

Chen HY, Chuan WS, Yu SB (1993) Network adjustment and precision estimation of the Taiwan GPS network (in Chinese), Proceedings of the 12th Surveying Conference of Taiwan, Chung-Li, Taiwan.
Cheney RE, Doyle NS, Douglas BC, Agreen RW, Miller I Timmerman EL, McAdoo DC (1991) The Complete Geosat Altimeter GDR Handbook, NOAA, Rockville, Maryland.
Cheney RE, Lillibridge JL (1992) ERS-1 fast deliver altimeter data for tropical ocean monitoring, EOS, Trans. AGU, 74 (14): 84
Dumont JP, Stum J (1994) Altimeter Products User Manual, C1-EX-MUT-A21-01-CN, issue 2.
Engelis T (1987) Radial Orbit Error Reduction and Sea Surface Topography Determination Using Satellite Altimetry, Dept. of Geodetic Science and Surveying, Rep. No. 377, The Ohio State University, Columbus.
Forsberg R (1984) A study of terrain reductions, density anomalies and geophysical inversion methods in gravity field modeling, Rep. No. 355, Dept. of Geod. Sci. and Surv., The Ohio State University, Columbus.
Glenn S, Robin A, Spall M (1987) Recent results from the Harvard Gulf Stream forecasting program, Oceanographic Monthly Summary, 7, No.4.
Haxby WF, Karner GD, LaBrecque JL, Weissel JK (1994) Digital Images of combined oceanic and continental data sets and their use in tectonic studies, EOS, Trans. AGU, 64.
Haines BJ, Born GH, Williamson RG, Koblinksky CJ (1994) Application of GEM-T2 gravity field to altimetric satellite orbit computation, J. Geophys. Res. 99: 16237–16254.
Heck B (1990) An evaluation of some systematic error sources affecting terrestrial gravity anomalies, Bull. Géod. 64:88–108.
Heiskanen W, Moritz H (1985) Physical Geodesy, reprint, Inst. of Phys. Geod., Technical University of Graz, Graz.
Hwang C (1989) High precision gravity anomaly and sea surface height estimation from Geos-3/Seasat altimeter data, Rep. No. 355, Dept. of Geod. Sci. and Surv., The Ohio State University, Columbus
Hwang C (1995) Orthonormal function approach for Geosat determination of sea surface topography, Marine Geodesy 18: 245–271
Hwang C, Parsons B (1995) Gravity anomalies derived from Seasat, Geosat, ERS-1 and TOPEX/POSEIDON altimetry and ship gravity: a case study over the Reykjanes Ridge, Geophy. J. Inst. 122:551–568
Hwang C, Parsons B (1996) An optimal procedure for deriving marine gravity from multi-satellite altimetry, Geophy. J. Int. 125: 705–719.
Hwang C (1996) A study of the Kuroshio's seasonal variabilities using an altimetric-gravimetric geoid and TOPEX/POSEIDON altimeter data, J. Geophys. Res. 101: 6313–6335.
Kahmen H, Faig W (1988) Surveying, Walter de Gruyter, Berlin
Kaula WM (1966) Theory of Satellite Geodesy, Blaisdell Publishing Co.,
Knudsen P (1991) Simultaneous estimation of the gravity field and sea surface topography from satellite altimeter data by least-squares collocation, Geophy. J. Int. 104: 307–317.
Levitus S (1982) Climatological Atlas of the World Ocean, NOAA Professional Paper 13, U.S. Dept. of Commerce, Rockville, Maryland.
Ma XC, Shum CK, Eanes RJ, Tapley BD (1994) Determination of ocean tides from the first year of TOPEX/POSEIDON altimeter measurements, J. Geophys. Res. 99: 24809–24820.
McAdoo DC, Marks K (1992) Gravity over the southern ocean from Geosat data, J. Geophys. Res. 97: 3247–3260.
Moritz H (1980) Advanced Physical Geodesy, Abacus Press, Karlsruhe.
Olgiati A, Balmino G, Sarrailh M, Green CM (1995) Gravity anomalies from satellite altimetry: comparison between computation via geoid heights and via deflections of the vertical, Bull. Géod. 69: 252–260.
Rapp RH (1982) A summary of the results from the OSU analysis of Seasat altimeter data, Rep. No. 335, Dept. of Geod. Sci. and Surv., The Ohio State University, Columbus.
Rapp RH (1989) Geometric Geodesy, vols I and II, Dept. of Geod. Sci. and Surv., The Ohio State University, Columbus.
Rapp RH, Wang WM, Pavlis NK (1991) The Ohio State 1991 geopotential model and sea surface topography harmonic coefficient model, Rep. No. 410, Dept. of Geod. Sci. and Surv., The Ohio State University, Columbus.
Rummel R (1993) Principle of satellite altimetry and elimination of radial orbit errors, in Rummel and Sanso (eds)., Lecture Notes in Earth Sciences, Vol. 50, Springer-Verlag, New York, pp. 189–241.
Sandwell DT, Zhang BH (1989) Global mesoscale variability from Geosat Exact Repeat Mission: correlation with ocean depth, J. Geophys. Res. 94: 17971–17984.
Sandwell DT (1992) Antarctic marine gravity field from high density satellite altimetry, Geophy. J. Int. 109:437–448.
Schwarz KP, Sideris MG, Forsberg R (1990) The use of FFT techniques in physical geodesy, Geophy. J. Int. 100:485–514.
Shih TY (1995) The study on GIS application for the gravity terrain correction and gravity estimation, Rep. No, NSC84-2211-E009-031, National Science Council of Rep. of China, Taipei.
Shum CK, Yuan DN, Ries JC, Smith JC, Schutz BE, Tapley BD (1994) Precision orbit determination for the Geosat Exact Repeat Mission, J. Geophys.Res. 95: 2887–2898.
Shum CK, Ries JC, Tapley BD (1995) The accuracy and applications of satellite altimetry, Geophy. J. Int. 121:321–336.
Smith WHF, Sandwell DT (1995) Marine gravity field from declassified Geosat and ERS-1 altimetry, paper presented at the 1995 Fall meeting of AGu, San Francisco.
Stewart RH (1985) Methods of Satellite Oceanography, University of California Press, Los Angeles.
Tai CK, Kuhn JM (1994) On reducing large scale time-dependent errors in satellite altimetry while preserving the ocean signal: orbit and tide error reduction for TOPEX/POSEIDON, NOAA TM NOS OES 009, Rockville, Maryland.
Tapley BD, Born GH, Parke ME (1982) The Seasat altimeter data and its accuracy assessment, J. Geophys. Res. 87: 3179–3188.
Tapley et al. (1994) Precision oribit determination for TOPEX/POSEIDON, J. Geophys. Res. 99: 24383–24404.
Torge W (1989) Gravimetry, Walter de Gruyter, Berlin.
Tschering CC, Rapp RH (1974) Closed covariance expressions for gravity anomalies, geoid undulations and deflections of the vertical implied by anomaly degree variance models, Rep. No. 410, Dept. of Geod. Sci. and Surv., The Ohio State University, Columbus.
Tsuei GC, Hsu TC, Lee HW, Wang WC (1993) Test of a gravimetric geoid using GPS traverse (in Chinese), Proceedings of the 12th Surveying Conference of Taiwan, Chung-Li, Taiwan.
Tsuei GC, Arabelos D, Forsberg R, Sideris MG, Tziavos IN (1994) Geoid computations in Taiwan, Proc. Joint meeting of the International Gravity and Geoid Commissions, Graz, in press.
Wang YM, Rapp RH (1990) Terrain effects on geoid undulation computations, manu. geodaetica 15: 23–29.
Wang YM, Rapp RH (1992) The determination of one year mean sea surface height track from Geosat altimeter data and ocena variability application, Bull. Géod. 66: 336–345
Williamson RG, Nerem RS (1994) Improved orbit computations for the Geosat mission: Benefits for the oceanographic and geodynamic studies, paper presented at the 1994 Fall meeting of AGU, San Francisco.
Yen HY, Yeh YH, Lin CH, Yu GK, Tsai YB (1990) Free-air gravity map of Taiwan and its applications, Terr., Atm. and Oceanic Sci. (TAO) 1: 143–156.